J Mater Sci (2015) 50:4422–4429
DOI 10.1007/s10853-015-9008-y

Mechanical properties of ultrafine-grained AlZnMg(Cu)-alloys AA7020 and AA7075 processed by accumulative roll bonding

M. Ruppert[1] · M. Strebl[1] · H. W. Höppel[1] · M. Göken[1]

Received: 13 February 2015 / Accepted: 1 April 2015 / Published online: 7 April 2015

Abstract Ultrafine-grained AA7020 (AlZnMg) and AA7075 (AlZnMgCu) were produced by accumulative roll bonding (ARB) with up to 6 cycles. Different pre-heating treatments and their effect on the mechanical performance of the materials were investigated by means of hardness measurements and uniaxial tensile testing. It was found for AA7020 that by pre-heating at 230 °C for 2.5 min prior to each rolling step, an UTS of 550 MPa can be achieved, which is 51 % higher compared to the peak-aged T6 reference. For AA7075, pre-heating at 280 °C for 2.5 min leads to a very high UTS of 720 MPa after four ARB passes. A negative strain rate sensitivity was found for both alloys, which shifts toward zero with increasing number of ARB cycles. Post-ARB heat treatment was performed in order to overcome the reduced ductility after ARB. This leads to an enhanced strain hardening capacity after 4 cycles, resulting in an increase of the uniform elongation from 1.4 to 2.0 % for AA7020 and from 0.9 to 2.1 % for AA7075.

Introduction

Severe plastic deformation (SPD) of technical aluminum alloys like 2000-, 6000-, or 7000-series alloys appears to have a high potential, as both precipitation strengthening and grain boundary strengthening can contribute to an increase in the mechanical properties of these wrought alloys [1]. From an industrial point of view, it is furthermore desirable to produce large amounts of bulk material. In this context, accumulative roll bonding (ARB) [2] seems to be very promising for continuous sheet production on established large-scaled manufacturing facilities [3–5]. Moreover, it was shown before that ARB leads to a significant increase in the mechanical properties, especially concerning strength and strain rate sensitivity [6–12]. Although there have been some studies about ARB processing of the precipitation hardenable 2000-series alloys like AA2219 [13, 14] or Al-2Cu [15] and several studies about ARB of 6000-series alloys like AA6014 [16], AA6016 [17], and AA6061 [18], there exist only few papers focusing on ARB of the high strength 7000-series. Hidalgo et al. studied the influence of the ARB-processing temperature on the microstructure, texture, and the hardness of AA7075 [19]. In that study, the ARB-process was conducted at 300, 350, and 400 °C, respectively. However, regarding the mechanical properties, it was found that the hardness of the ARB-processed material is lower than that of the initial material in T6-condition, due to particle coarsening. In another study by Hidalgo-Manrique et al. [20] AA7075 was processed at 300 °C by a 3:1 thickness reduction per cycle, up to 5 ARB cycles. The microstructure was found to be composed of equiaxed grains and subgrains with a mean size of 355 nm. Furthermore, uniaxial tensile tests performed at 300 °C indicated superplastic behavior for N4 samples, similar to the results in [21]. Another study by Hidalgo-Manrique et al. [22] on the same system focuses on the influence of the processing temperature on the particle pinning effect and therefore on the achievable mean crystallite size and misorientation. However, there are no data available that focus on the improvement of the mechanical properties of 7000-series alloys at room

✉ M. Ruppert
mathis.ruppert@ww.uni-erlangen.de;
http://www.gmp.ww.uni-erlangen.de

[1] Department of Materials Science and Engineering, Institute I: General Materials Properties, Friedrich-Alexander-University of Erlangen-Nürnberg, Martensstr. 5, 91058 Erlangen, Germany

temperature due to ARB and an optimization of the processing conditions.

In this study, the commercially available aluminum alloys AA7020 and AA7075 were processed by ARB under various pre-heating conditions up to 6 ARB cycles. Hardness measurements were conducted in order to identify the most favorable processing conditions concerning bonding and mechanical properties. Subsequently, uniaxial tensile testing was performed at room temperature at different strain rates. The impact on the mechanical properties of a post-ARB heat treatment, which can be compared to a typical paint-bake sequence known from automotive industry, was also analyzed.

Experimental

The AlZnMg(Cu)-alloys AA7020 and AA7075 were used as initial sheet material. The chemical compositions of these materials are given in Table 1.

Sample sheets were kindly provided by AMAG Austria Metall AG in T6-condition and had an initial geometry of 100 × 150 × 2.5 mm (width × length × thickness) for AA7020 and 100 × 200 × 1.5 mm for AA7075. The sheets were rolled down to 1-mm thickness and afterward heat-treated at 480 °C for 1 h and quenched in water. Henceforth, this condition is denoted as N0. A four high rolling mill was used at room temperature and at a rolling velocity of 1 m/min for ARB processing. The sheets were degreased in acetone and wire brushed with a rotating steel brush to remove the oxide layer. In order to optimize the processing parameters, the sheets were supplied to different pre-heating conditions prior to each rolling step, which are listed in Table 2.

In each case, rolling of the sheets was performed instantly after the heating sequence with a thickness reduction of 50 %. If sufficient bonding was achieved, the sheet was cut in two halves, and the procedure was repeated as described above. Microstructural characterization was conducted in rolling plane using a Zeiss Cross Beam 1540 EsB (Carl Zeiss AG, Oberkochen, Germany) scanning electron microscope in backscattered electron contrast. Median grain size was determined by means of line intersection method and calculating the cumulative frequency of the grain size distribution. Thereby, the value at 50 % equals the median grain size. It has to be noted that no distinction between low- and high-angle grain boundaries was made. Moreover, the mechanical properties of the produced samples were determined. Therefore, Vickers hardness HV5 was measured using a LECO 100A in order to study the influence of different pre-heating parameters and the thermal stability of the samples. Furthermore, tensile testing was performed in rolling direction, using an Instron 4505 universal testing machine at room temperature and strain rates of 10^{-3} and 10^{-5} s^{-1}, respectively.

Table 1 Chemical compositions of AA7020 and AA7075 in wt%

Alloy	Chemical composition in wt%								
	Fe	Si	Cu	Mn	Mg	Cr	Zn	Ti	Zr
AA7020	0.28	0.18	0.12	0.17	1.11	0.12	4.53	0.03	0.09
AA7075	0.13	0.07	1.50	0.02	2.69	0.19	5.83	0.04	

The data were provided by AMAG Austria Metall AG

Table 2 Pre-heating conditions and maximum number of ARB cycles with sufficient bonding

Alloy	Temperature (°C)	Time (min)	ARB cycles
AA7020	Room temperature	–	6
	180	2.5	6
	230	2.5	6
	280	2.5	6
AA7075	Room temperature	–	No bonding
	230	2.5	2
	280	2.5	4
	300	5	6

Results and discussion

The effect of varying pre-heating temperature and time on the mechanical properties and the achievable number of ARB cycles with sufficient bonding was studied according to Table 2. The results of the hardness measurements for AA7020 and AA7075 after different numbers of ARB cycles are shown in Fig. 1 for the various pre-heating conditions.

Alloy AA7020 shows a strong increase in hardness with the number of ARB cycles. Already after one ARB cycle the hardness of the T6 condition is reached. For pre-heating treatments at 230 °C/2.5 min and 280 °C/2.5 min, the hardness reaches a maximum at N5, while it increases between N5 and N6 for RT and 180 °C/2.5 min. After 6 cycles, all pre-heating conditions result in the same hardness, except for 280 °C/2.5 min which is slightly reduced due to grain coarsening and overaging, respectively. Although sufficient bonding was achieved already at RT and at 180 °C strong necking at the sheet edge appeared after 2 cycles. This was slightly reduced at higher pre-heating temperatures. For AA7075, bonding of the sheets could not be achieved at temperatures below 230 °C. As AA7075 exhibits a higher content of alloying elements compared to AA7020, higher temperatures are necessary to achieve good bonding [23]. Thereby, the addition of Cu

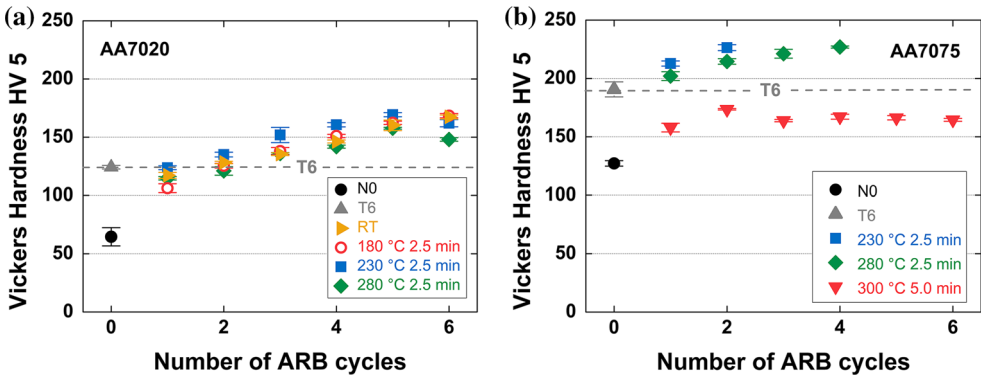

Fig. 1 Vickers hardness HV5 versus the number of ARB cycles for **a** AA7020 and **b** AA7075 using different pre-heating parameters. As a reference, the hardness in T6-condition is plotted

and the higher amount of Zn and Mg increase the hardness and the strength of AA7075 compared to AA7020, due to decreased solubility of Zn in the Al matrix and an increased aging rate. Because of the lower hardness of AA7020, higher surface roughness could be achieved by wire brushing, which promotes bonding [24]. Both for 230 and 280 °C a strong hardness increase was found after the first cycle. Despite the higher hardness of the samples which were pre-heated at 230 °C, sufficient bonding could only be achieved up to two cycles of ARB. Therefore, the best combination of hardness and bond strength was found after pre-heating the samples at 280 °C for 2.5 min prior to the rolling procedure. Moreover, pre-heating at 300 °C/5 min leads to smaller hardness compared to the T6-condition, which is in agreement with the results of Hidalgo et al. [19]. On the one hand, this is due to overaging; on the other hand, the comparatively high temperatures promote recovery and grain coarsening at the expense of grain refinement by ARB.

In Fig. 2, SEM micrographs for both alloys are shown in T6 condition and representatively after 4 ARB cycles, respectively. The grain size in T6 condition for AA7020 was found to be 25 µm in rolling direction and 10.5 µm in normal direction, corresponding to an aspect ratio of 2.4. After heat treatment, the grains became more equiaxed in N0 condition, and an aspect ratio of 1.8 was found. This aspect ratio increased with the number of ARB cycles up to 4.1 after 6 cycles of ARB at 230 °C/2.5 min. Therefore, a median grain size of 616 nm in rolling direction and 150 nm perpendicular to this direction was found. In contrast to that, AA7075 reveals a rather inhomogeneous microstructure after ARB processing (280 °C/2.5 min). That is to say, it is in an early ARB state, characterized by a deformation structure with no clear grain boundaries. The differences in the microstructural evolution of both alloys are due to the different processing temperatures. Therefore, the higher pre-heating temperature used for AA7075 leads to less accumulated strain by pronounced recovery and precipitation growth during the heating sequences prior to roll bonding. Based on the results from hardness measurements, tensile tests were conducted on ARB samples processed under different pre-heating conditions. Stress–strain curves for AA7020 are shown in Fig. 3a for the initial N0 condition, the T6-condition and the ARB-processed samples which were pre-heated at 230 °C for 2.5 min. Moreover, samples processed at pre-heating conditions of 300 °C/5 min, which are similar to the process parameters of Hidalgo et al. [19], are also plotted as a reference. T6-condition shows a very good combination of strength and ductility. That is to say, an UTS of 360 MPa and an elongation to failure of 22 % are reached. After the heat treatment, the UTS decreases to 270 MPa and only a slight increase in terms of elongation to failure; however, an enormous increase in terms of uniform elongation from 7 to 19 % is visible. With increasing ARB cycles, both yield strength and ultimate tensile strength are increasing again and exceed T6-condition already after N2 cycles of ARB. However, simultaneously, both uniform elongation and elongation to failure are reduced with increasing ARB cycles. After 6 cycles of ARB an UTS of 550 MPa is reached. Nevertheless, it is also observed that some samples fractured early due to a weak bond strength of the last bonding plane after N6. For 300 °C/5 min after N4, strength does not show a significant improvement compared to T6-condition, however, the ductility decreased distinctly. Generally, a similar trend can be found for AA7075, see Fig. 3b. However, for ARB samples processed with pre-heating conditions of 280 °C/2.5 min, UTS of T6 is already exceeded after N1 and an UTS of 720 MPa is reached after N4. Moreover, Fig. 3c reveals that both for AA7020 and for AA7075 no saturation in strength is reached after N4 and N6, respectively. For AA7020, a total increase in UTS by 51 % compared to the T6 condition is found. Nonetheless, Fig. 3d shows that the uniform elongation decreased by 84 % after 6 ARB cycles. Furthermore, AA7075 reveals an increase of the UTS by 22 % accompanied by a decrease of the uniform elongation by 90 %.

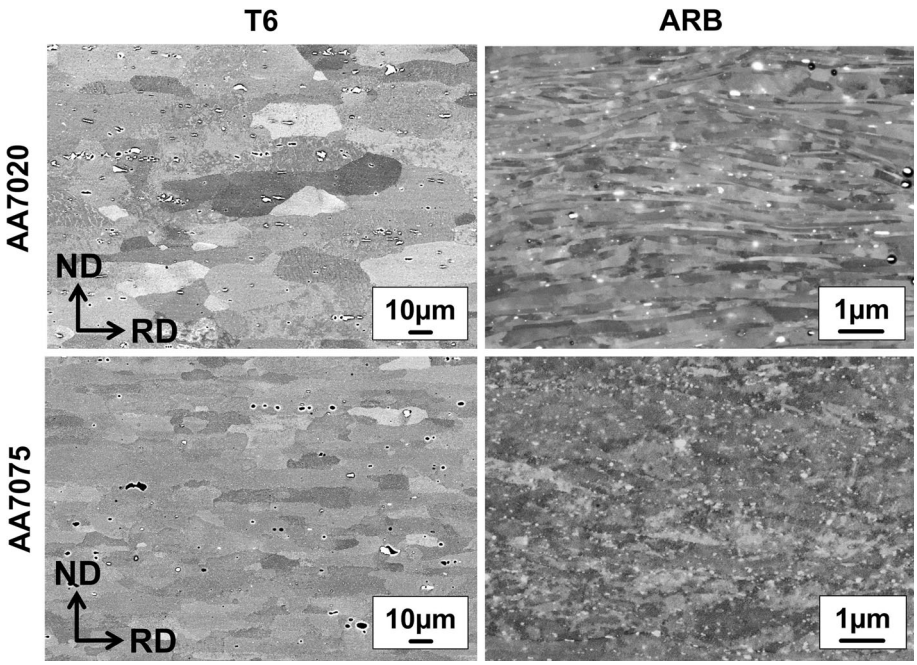

Fig. 2 SEM micrographs in BSE contrast for AA7020 (230 °C/2.5 min) and AA7075 (280 °C/2.5 min) in T6-condition and after ARB processing up to N4

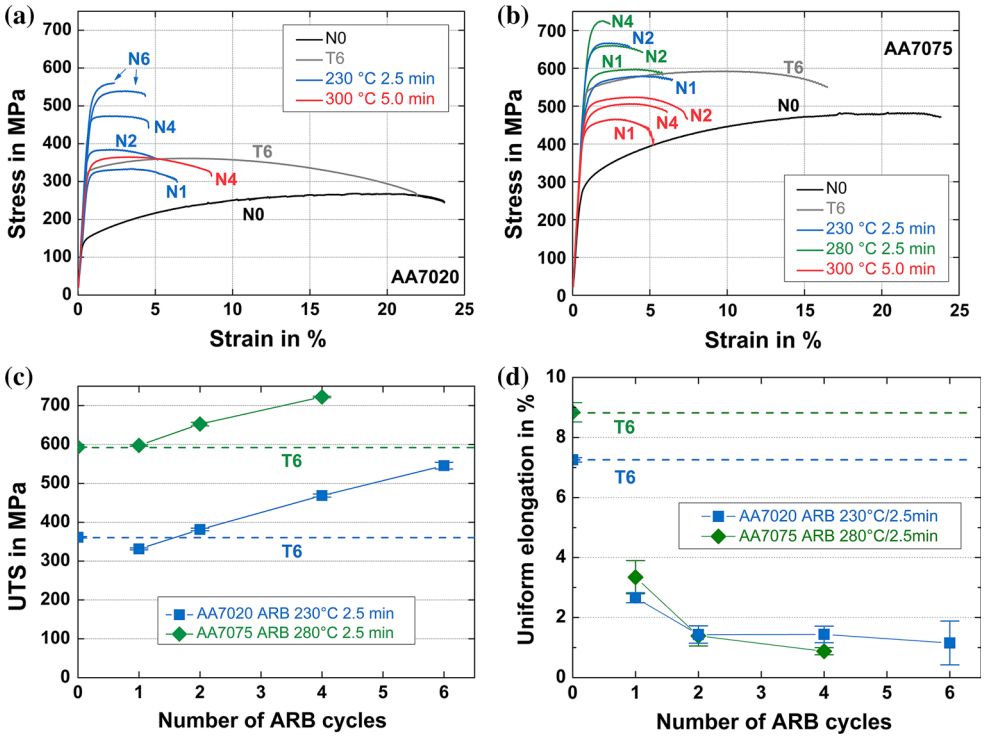

Fig. 3 Stress–strain diagrams for **a** AA7020 and **b** AA7075 after different numbers of ARB cycles and different pre-heating conditions. As a reference, T6-condition is plotted. **c** UTS and **d** Uniform elongation versus ARB cycles compared for AA7020 after ARB at 230 °C/2.5 min, AA7075 after ARB at 280 °C/2.5 min, and the T6-condition for both the alloys

The results from tensile testing in terms of decreasing ductility with increasing number of ARB cycles are typical for most alloys after SPD, due to a reduction of strain hardening capacity. However, Höppel et al. [9] reported increasing strength and ductility for ARB-processed UFG Al99.5 compared to its cold-rolled counterpart. The found behavior could be explained by an enhanced strain rate sensitivity (SRS) of this material after ARB processing. Furthermore, Hausöl et al. [25] found an increasing elongation to failure with increasing number of ARB cycles for the AlMgSi-alloy AA6014. In accordance to the aforementioned behavior, Vevecka et al. [26] found also increased strain rate sensitivity of the AlMgSi-alloy AA6061 after ECAP. Similar observations of increasing ductility

with the number of ARB cycles are also found for other aluminum alloys of the 3000 series [27, 28], the 6000 series [17], and the 8000 series [29, 30].

In order to quantify the strain rate sensitivity of the materials used in this study, tensile testing at room temperature was performed in N0, N2, and N4 condition at strain rates of 10^{-3} and 10^{-5} s^{-1} shown in Fig. 4. The SRS was determined according to Hart et al. [31]. However, as a microstructural stable condition is hardly achieved during tensile testing, the stress–strain curves were analyzed at maximum stress, which appears to be a good compromise between the evolution of the microstructure and the limitations of the onset of necking. For all samples, an increase in the strain hardening capacity is found at lower strain rates. However, the YS remains rather constant. Although AA7020 N4 shows a lower YS at a strain rate of 10^{-5} s^{-1}, the sample reaches the same UTS, due to an increased strain hardening capacity. Moreover, the uniform elongation is doubled after N4 when the strain rate is decreased, while the elongation to failure increases from 3.5 to 6.0 %. The results for AA7020 indicate a negative strain rate sensitivity of $m = -0.0195$, which shifts toward 0 with increasing number of ARB cycles. Likewise for AA7075 also a more pronounced strain hardening behavior is observed at lower strain rates. Furthermore, the uniform elongation and the elongation to failure are increasing with decreasing strain rate. This behavior is in good accordance with observations by Dorward et al. [32], who found an increasing UTS, uniform elongation, and elongation to failure for CG AA7075 in O-condition while decreasing the strain rate from 10^{-1} to 10^{-3} s^{-1}. Additionally, also a negative strain rate sensitivity of $m = -0.0063$ was found for N0, which increases with the number of ARB cycles and reaches a value of $m = -0.0032$ after N4. On the one hand, enhanced SRS is frequently observed during SPD, as the fraction of high-angle boundaries is increasing with the number of SPD cycles [33]. According to Blum et al. [34], those high-angle boundaries act as sources and sinks for dislocations. Consequently, an increased fraction of high-angle boundaries leads to an increased interaction activity of dislocations by thermally activated annihilation of dislocations [35]. As this process is diffusion controlled, the dislocation density in the grain volume is strongly influenced by the applied strain rate. As the microstructural evolution for AA7020 is faster compared to AA7075, the increase in the fraction of high-angle boundaries is also higher. Hence, the increment in SRS of AA7020 is quicker compared to AA7075. On the other hand, both negative strain rate sensitivity and the Portevin–Le Châtelier effect [36] are macroscopic manifestations of dynamic strain aging, which means that dislocations are pinned at less mobile solute atoms. In the solution annealed N0 condition, the concentration of solute atoms in the matrix is rather high leading to pronounced dynamic strain aging. With increasing number of ARB cycles, the amount of solute atoms however is decreasing due to precipitation during the heating sequences and the rolling procedure. As an effect of an increasing fraction of high-angle boundaries and a decreasing content of mobile solute atoms, the SRS is increasing with the number of ARB cycles, but still remains

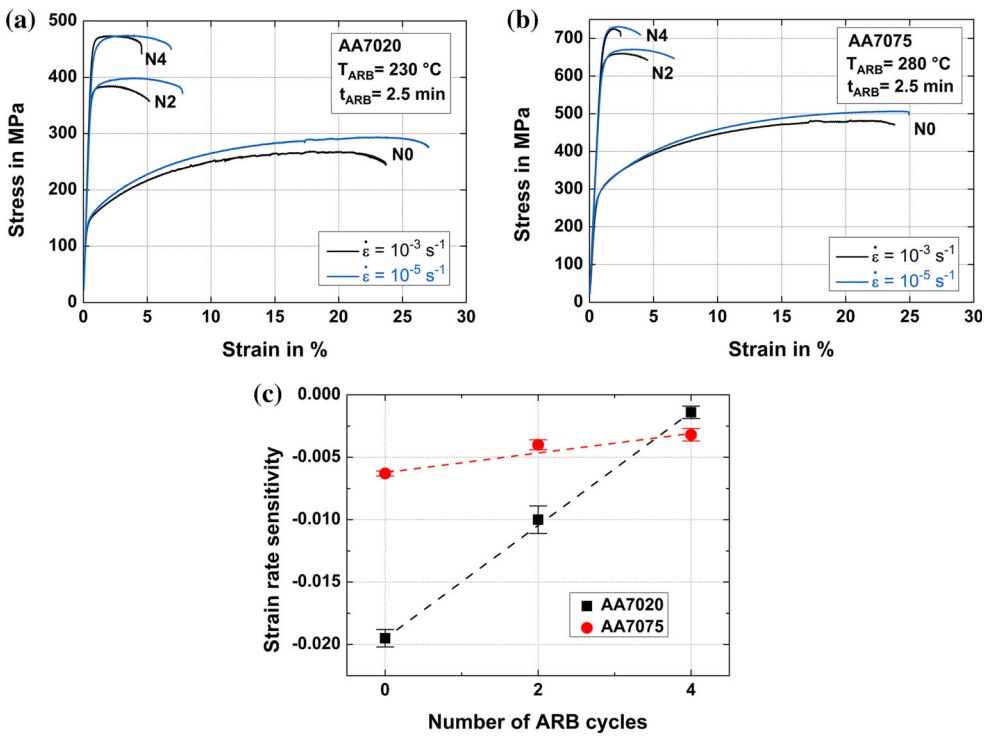

Fig. 4 Stress–strain curves for **a** AA7020 and **b** AA7075 at strain rates of 10^{-3} and 10^{-5} s^{-1} at RT. **c** Strain rate sensitivity versus the number of ARB cycles for both the alloys

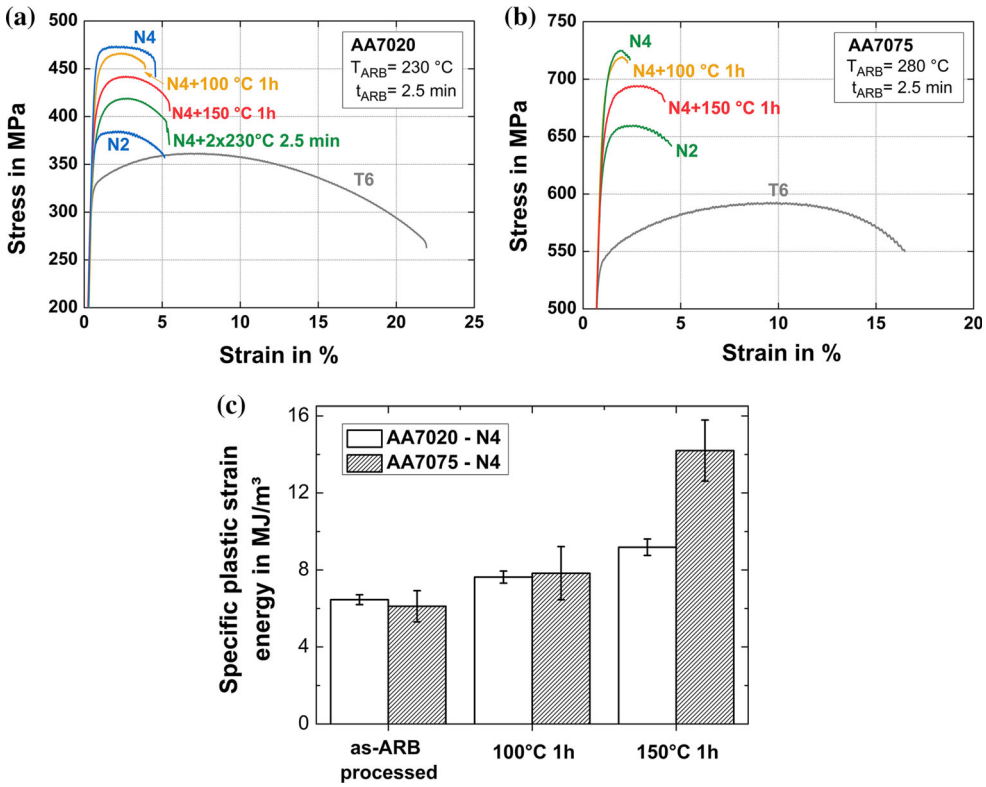

Fig. 5 Stress–strain diagrams after post-ARB heat treatment for **a** AA7020 and **b** AA7075. **c** Specific plastic strain energy in MJ/m^3 until uniform elongation for the as-ARB-processed N4 condition and after heat treatment

negative. Moreover, Kapoor et al. [37] found that SPD of Al–1.5 Mg using equal channel angular pressing results in shifting the domain of negative strain rate sensitivity, which fits the behavior found in this study for AlZnMg. That is to say, the conventionally grained material shows a more negative SRS compared to the UFG counterpart. Furthermore, it is supposed that only positive strain rate sensitivity after SPD processing can lead to the aforementioned "paradoxon of strength and ductility" [7] found in literature. However, the investigated 7000 series alloys show negative strain rate sensitivity. Additionally, Hausöl et al. [25] found also decreasing ductility with increasing number of ARB cycles for a 5000-series alloy, which are also known to show a negative strain rate sensitivity [38, 39].

In order to overcome the drawback of a reduced ductility after rolling and to simulate a common paint-bake sequence which is usually done in automotive industry, post-ARB heat treatment was performed for N4 samples of both the alloys. The effect of a post-ECAP heat treatment on the mechanical properties of AA7075 was already studied before by Fritsch et al. [40], where ECAP processing was performed at cryogenic temperatures. Hockauf et al. [41] also reported the positive influence of a post-ECAP heat treatment on the ductility of an ultrafine-grained Al–Mg–Si alloy before, which was especially pronounced at a lower number of ECAP passes. The results indicate a high potential for improvements by post-ARB heat treatments of 7000-series alloys after ARB processing. Some representative results from the present study are shown in Fig. 5 for AA7020 and AA7075. In terms of AA7020, a heat treatment at 150 °C for 1 h leads to a decrease of the YS from 450 to 402 MPa and of the UTS from 468 to 442 MPa. That is to say, the relative decrease in YS is much higher than the decrease in UTS, which means that the strain hardening capacity increased by the post-ARB heat treatment. From Fig. 3c, it can be derived that the microstructural evolution [33] has not saturated yet after N4, as there is also no saturation in the mechanical properties visible. As reported by Topic et al. [17], precipitates in ultrafine-grained alloys can further retard dynamic recovery during ARB. Therefore, the saturation of the mechanical properties is shifted to higher strains and after lower numbers of ARB cycles still a very high dislocation density in the grain interior can be found. Due to the post-ARB heat treatment, dislocations can recover at grain boundaries, leading to an increase in strain hardening capacity. This also leads to an increase in uniform elongation of N4 samples from 1.4 to 2.0 % for AA7020. Moreover, an increase of the elongation to failure from 3.2 to 4.2 % and therefore an improvement of the combination of strength and ductility compared to the N4 condition directly after ARB could be achieved. The post-ARB heat treatment at 100 °C/1 h does not lead to pronounced recovery and therefore no increase in ductility, while for 2 × 230 °C/2.5 min, the thermal stability of the UFG alloy

is exceeded. Hence, the heat treatment at 150 °C/1 h leads to the most favorable results. This improved combination can also be derived by calculating the area under the stress–strain curves. Therefore, Fig. 5c shows the specific plastic strain energy until the uniform elongation for the as-ARB-processed N4 condition and the heat-treated samples. A similar trend as described above can also be found for AA7075. That is to say, for N4 the YS and the UTS decrease after heat treatment at 150 °C for 1 h, from 687 to 647 MPa and from 722 to 693 MPa, respectively. However, the uniform elongation increases from 0.9 to 2.1 %, and the elongation to failure increases from 1.5 to 3.3 %. Thus, by analogy with AA7020, the combination of strength and ductility can be enhanced compared to the as-ARB-processed condition.

Although the post-ARB heat treatment could clearly improve the ductility of the investigated alloys while maintaining high strength compared to the as-ARB-processed state, the achieved ductility is still rather small. Especially, the elongation to failure seems to be strongly reduced during ARB processing. One possible approach in order to further ameliorate the elongation to failure could be an enhancement of the bond strength of the samples, as necking of individual sheet layers could be suppressed. Therefore, an increased thickness reduction during sheet production might have a positive effect [42]. Moreover, processing at cryogenic temperatures could suppress dynamic recovery, which could result in an increase of the strain hardening capacity and in the suppression of strain localization [40].

Conclusions

Ultrafine-grained sheets of AA7020 (AlZnMg) and AA7075 (AlZnMgCu) were processed by ARB at various pre-heating conditions. In order to quantify the most favorable combination of ARB processing conditions to achieve sufficient bonding and mechanical performance, hardness measurements and uniaxial tensile testing at different strain rates were performed. Furthermore, a post-ARB heat treatment was conducted in order to optimize the combination of strength and ductility. The following results have been obtained:

- Among the investigated pre-heating conditions, 230 °C/2.5 min and 280 °C/2.5 min lead to the most favorable combination of strength and sufficient bonding for AA7020 and AA7075, respectively. Therefore, an UTS of 550 MPa could be achieved for AA7020 after N6 and 720 MPa after N4 for AA7075.
- A post-ARB heat treatment at 150 °C could enhance the combination of strength and ductility for both the alloys. While the UTS decreased only slightly by 6 % for AA7020 and by 4 % for AA7075 during the heating sequence, the uniform elongation increased by 40 % for AA7020 and by 120 % for AA7075 compared to the as-ARB-processed condition. However, in order to achieve enhanced ductility of ultrafine-grained 7xxx-series alloys, further attempts are necessary.
- Moreover, tensile testing at lower strain rates leads to an increase in strain hardening capability for both the alloys. A negative strain rate sensitivity was found for the processed samples, which shifts toward zero with increasing number of ARB cycles.

Acknowledgements The authors gratefully acknowledge the financial support of the German Research Council (DFG) und project GO 741/19-1 and the Cluster of Excellence "Engineering of Advanced Materials" Erlangen-Nürnberg which is funded within the framework of its "Excellence Initiative." Furthermore, the authors would especially like to thank Werner Fragner from AMAG Austria Metall AG for providing the sheet material.

References

1. Zhao YH, Liao XZ, Zhu YT, Valiev RZ (2004) Enhanced mechanical properties in ultrafine grained 7075 Al alloy. J Mater Res 20:288–291. doi:10.1557/JMR.2005.0057
2. Saito Y, Tsuji N, Utsunomiya H, Sakai T, Hong RG (1998) Ultrafine grained bulk aluminum produced by accumulative roll-bonding (ARB) process. Scr Mater 39:1221–1227. doi:10.1016/S1359-6462(98)00302-9
3. Tsuji N, Saito Y, Lee SH, Minamino Y (2003) ARB (accumulative roll-bonding) and other new techniques to produce bulk ultrafine grained materials. Adv Eng Mater 5:338–344. doi:10.1002/adem.200310077
4. Tsuji N, Ito Y, Nakashima H, Yoshida F, Minamino Y (2002) Change in microstructure during annealing of ultrafine grained aluminum produced by ARB. Mater Sci Forum 396–402:423–428. doi:10.4028/www.scientific.net/MSF.396-402.423
5. Ruppert M, Böhm W, Nguyen H, Höppel HW, Merklein M, Göken M (2013) Influence of upscaling accumulative roll bonding on the homogeneity and mechanical properties of AA1050A. J Mater Sci 48:8377–8385. doi:10.1007/s10853-013-7648-3
6. Lowe TC, Valiev RZ (2000) Producing nanoscale microstructures through severe plastic deformation. JOM 52:27–28. doi:10.1007/s11837-000-0127-8
7. Valiev RZ, Alexandrov IV, Zhu YT, Lowe TC (2002) Paradox of strength and ductility in metals processed by severe plastic deformation. J Mater Res 17:5–8. doi:10.1557/JMR.2002.0002
8. Höppel HW, Valiev RZ (2002) On the possibilities to enhance the fatigue properties of ultrafine-grained metals. Z Metall 93:641–648. doi:10.3139/146.020641
9. Höppel HW, May J, Göken M (2004) Enhanced strength and ductility in ultrafine-grained aluminium produced by accumulative roll bonding. Adv Eng Mater 6:781–784. doi:10.1002/adem.200306582
10. May J, Höppel HW, Göken M (2005) Strain rate sensitivity of ultrafine-grained aluminium processed by severe plastic deformation. Scr. Mater. 53:189–194. doi:10.1016/j.scriptamat.2005.03.043
11. Tsuji N, Saito Y, Utsunomiya H, Tanigawa S (1999) Ultra-fine grained bulk steel produced by accumulative roll-bonding (ARB)

process. Scr Mater 40:795–800. doi:10.1016/S1359-6462(99)00015-9
12. Wei Q (2007) Strain rate effects in the ultrafine grain and nanocrystalline regimes—influence on some constitutive responses. J Mater Sci 42:1709–1727. doi:10.1007/s10853-006-0700-9
13. Roy S, Nataraj BR, Suwas S, Kumar S, Chattopadhyay K (2012) Accumulative roll bonding of aluminum alloys 2219/5086 laminates: Microstructural evolution and tensile properties. Mater Des 36:529–539. doi:10.1016/j.matdes.2011.11.015
14. Roy S, Nataraj BR, Suwas S, Kumar S, Chattopadhyay K (2012) Microstructure and texture evolution during accumulative roll bonding of aluminium alloys AA2219/AA5086 composite laminates. J Mater Sci 47:6402–6419. doi:10.1007/s10853-012-6567-z
15. Tsuji N, Iwata T, Sato M, Fujimoto S, Minamino Y (2004) Aging behavior of ultrafine grained Al–2 wt%Cu alloy severely deformed by accumulative roll bonding. Sci Technol Adv Mater 5:173–180. doi:10.1016/j.stam.2003.10.019
16. Hausöl T, Höppel HW, Göken M (2010) Tailoring materials properties of UFG aluminium alloys by accumulative roll bonded sandwich-like sheets. J Mater Sci 45:4733–4738. doi:10.1007/s10853-010-4678-y
17. Topic I, Höppel HW, Göken M (2007) Deformation behaviour, microstructure and processing of ARB aluminium alloy AA6016. Int J Mater Res 98:320–324. doi:10.3139/146.101469
18. Lee SH, Saito Y, Sakai T, Utsunomiya H (2002) Microstructures and mechanical properties of 6061 aluminum alloy processed by accumulative roll-bonding. Mater Sci Eng A 325:228–235. doi:10.1016/S0921-5093(01)01416-2
19. Hidalgo P, Cepeda-Jiménez CM, Ruano OA, Carreño F (2010) Influence of the processing temperature on the microstructure, texture, and hardness of the 7075 aluminum alloy fabricated by accumulative roll bonding. Metall Mater Trans A 41:758–767. doi:10.1007/s11661-009-0138-1
20. Hidalgo P, Cepeda-Jiménez CM, Ruano OA, Carreño F (2012) Effect of warm accumulative roll bonding on the evolution of microstructure, texture and creep properties in the 7075 aluminium alloy. Mater Sci Eng A 556:287–294. doi:10.1016/j.msea.2012.06.089
21. Hidalgo P, Cepeda-Jiménez CM, Orozoco-Caballero A, Ruano OA, Carreño F (2014) Evolution of the microstructure, texture and creep properties of the 7075 aluminium alloy during hot accumulative roll bonding. Mater Sci Eng A 606:434–442. doi:10.1016/j.msea.2014.03.105
22. Hidalgo P, Cepeda-Jiménez CM, Orozoco-Caballero A, Ruano OA, Carreño F (2014) Role of particles on microstructure and mechanical properties of the severely processed 7075 aluminium alloy. J Mater Sci 49:833–841. doi:10.1007/s10853-013-7767-x
23. Li L, Nagai K, Yin F (2008) Progress in cold roll bonding of metals. Sci Technol Adv Mater 9:1–11. doi:10.1088/1468-6996/9/2/023001
24. Tylecote RF, Howd D, Furmidge JE (1958) The influence of surface films on the pressure welding of metals. Br Weld J 5:21–38
25. Hausöl T, Höppel HW, Göken M (2011) Microstructure and mechanical properties of accumulative roll bonded AA6014/5754 aluminium laminates. Mater Sci Forum 667–669:217–222. doi:10.4028/www.scientific.net/MSF.667-669.217
26. Vevecka-Priftaj A, Böhner A, May J, Höppel HW, Göken M (2008) Strain rate sensitivity of ultrafine grained aluminium alloy AA6061. Mater Sci Forum 584–586:741–747. doi:10.4028/www.scientific.net/MSF.584-586.741
27. Xing ZP, Kang SB, Kim HW (2002) Structure and properties of AA3003 alloy produced by accumulative roll bonding process. J Mater Sci 37:717–722. doi:10.1023/A:1013879528697
28. Wei KX, Wei W, Du QB, Hu J (2009) Microstructure and tensile properties of Al–Mn alloy processed by accumulative roll bonding. Mater Sci Eng A 525:55. doi:10.1016/j.msea.2009.06.028
29. Kim HW, Kang SB, Tsuji N, Minamino Y (2005) Elongation increase in ultrafine-grained Al–Fe–Si alloy sheets. Acta Mater 53:1737–1749. doi:10.1016/j.actamat.2004.12.022
30. Xing ZP, Kang SB, Kim HW (2002) Microstructural evolution and mechanical properties of the AA8011 alloy during the accumulative roll-bonding process. Metall Mater Trans A 33:1521–1530. doi:10.1007/s11661-002-0074-9
31. Hart EW (1967) Theory of the tensile test. Acta Metall 15:351–355. doi:10.1016/0001-6160(67)90211-8
32. Dorward RC, Hasse KR (1995) Strain rate effects on tensile deformation of 2024-O and 7075-O aluminum alloy sheet. J Mater Eng Perform 4:216–220. doi:10.1007/BF02664116
33. Huang X, Tsuji N, Hansen N, Minamino Y (2003) Microstructural evolution during accumulative roll-bonding of commercial purity aluminum. Mater Sci Eng A 340:265–271. doi:10.1016/S0921-5093(02)00182-X
34. Blum W, Zeng XH (2009) A simple dislocation model of deformation resistance of ultrafine-grained materials explaining Hall–Petch strengthening and enhanced strain rate sensitivity. Acta Mater 57:1966–1974. doi:10.1016/j.actamat.2008.12.041
35. Li YZ, Zeng XH, Blum W (2004) Transition from strengthening to softening by grain boundaries in ultrafine-grained Cu. Acta Mater 52:5009–5018. doi:10.1016/j.actamat.2004.07.003
36. Penning P (1972) Mathematics of the Portevin–Le Chatelier effect. Acta Metall 20:1169–1175. doi:10.1016/0001-6160(72)90165-4
37. Kapoor R, Gupta C, Sharma G, Chakravartty JK (2005) Deformation behavior of Al–1.5Mg processed using the equal channel angular pressing technique. Scr Mater 53:1389–1393. doi:10.1016/j.scriptamat.2005.08.026
38. Král R, Lukác Janecek M (1996) Critical conditions for Portevin–Le Châtelier instabilities in Al–4.8%Mg and Al–2.57%Mg alloys. Mater Sci Forum 217–222:1025–1030. doi:10.4028/www.scientific.net/MSF.217-222.1025
39. Picu RC, Vincze G, Ozturk F, Gracio JJ, Barlat F, Maniatty AM (2005) Strain rate sensitivity of the commercial aluminum alloy AA5182-O. Mater Sci Eng A 390:334. doi:10.1016/j.msea.2004.08.029
40. Fritsch S, Scholze M, Wagner MFX (2012) Cryogenic forming of AA7075 by equal-channel angular pressing. Materialwiss Werkstofftech 43:561–566. doi:10.1002/mawe.201200001
41. Hockauf M, Meyer LW, Zillmann B, Hietschold M, Schulze S, Krüger L (2009) Simultaneous improvement of strength and ductility of Al–Mg–Si alloys by combining equal-channel angular extrusion with subsequent high-temperature short-time aging. Mater Sci Eng A 503:167–171. doi:10.1016/j.msea.2008.02.051
42. Vaidyanath LR, Nicholas MG, Milner DR (1958) Pressure welding by rolling. Br Weld J 6:13–28